Jour. of the KGS, Vol. 20, No. 2. March 2004, pp. 37~46

Numerical Analysis of Confining Effect Due to Geosynthetics Wrapping Compacted Soil Specimen

토목섬유로 보강된 다짐토 공시체의 구속효과에 관한 수치계산

Kim, Eun-Ra[1] 김 은 라
Kang, Ho-Keun[2] 강 호 근

요 지

본 연구에서는 토목섬유로 보강된 다짐토의 메카니즘이 제시되며, 이러한 메카니즘은 다짐토의 체적팽창(다일러턴시)을 토목섬유에 의해 구속 억제하는 과정에서 생성되는 효과로 간주된다. 먼저, 실내실험을 위한 구체적인 방법으로서, 토목섬유의 보강효과를 정량적으로 파악하기 위하여 사질토를 다짐하여 공시체를 만들어 그 주위에 토목섬유를 설치한 후 전체적으로 압축전단시험을 실시하였다. 실험에서 초기 다짐도는 각각의 종류에 대하여 다일러턴시의 특성이 다르기 때문에 각각의 공시체에 대하여 변화시켰다. 여기서 전단시험 도중에 다짐토의 다일러턴시 변형을 방지하기 위한 토목섬유에 작용하는 축방향 힘들(axial forces)이 조사되었다. 또한 다짐토의 탄소성 모델과 이러한 모델에 필요한 초기 입력치 값의 결정 방법들이 제시된다. 마지막으로, 탄소성 구성 모델에서 항복 이전의 탄성영역의 거동을 모사하기 위하여 Hashiguch(1989)가 제안한 subloading surface의 개념을 도입하여, 유한요소(FEM)해석을 통해 얻어진 결과들을 실내시험의 결과와 비교 분석하였다.

Abstract

This paper presents the modeling of geosynthetic-reinforced soils and discusses the reinforcement effect arising from confining the dilatancy deformation of the soil by geosynthetics. A series of compressive shear tests for compacted sandy soil specimens wrapped by geosynthetics are carried out by quantitatively examining the geosynthetic-reinforcement effect, and it occurred from the confinement of the dilative deformation of compacted soils during shearing. In the test, the initial degree of compaction is changed for each series of sandy soil specimens so that each series has different degree of dilatancy characteristics. Herein, the axial forces working to the geosynthetics so as to prevent dilative deformation of compacted soils during shearing are measured. Furthermore, the elasto-plastic modeling of compacted soils and a rational determination procedure of input parameters needed in the elasto-plastic modeling are presented. In this paper, the subloading yielding surface(Hashiguchi(1989)) is introduced to the elasto-plastic modeling which could describe the irreversible deformation characteristics of compacted soils during shearing. Finally, the elasto-plastic finite element simulation is carried out and the geosynthetic-reinforcement effect is discussed.

Keywords : Compacted soils, Elasto-plastic modeling, Geosynthetic-reinforcement

1 Member, Dept., of Civil Eng., Chonbuk National Univ. (kimeunra@chonbuk.ac.kr)
2 Ph.D. School of Mechanical and Aerospace, Gyeongsang National Univ.

1. Introduction

The geosynthetic-reinforced soil structures consist of two elements: one is compacted soil and the other is geosynthetics. The reinforcing effect should not be interpreted that the strength and rigidity of soil itself are merely supplemented by geosynthetic-reinforcement but be understood that soils and the geosynthetics are unified and show their fresh strength and rigidity as a composite material. The strength and rigidity of geosynthetic-reinforced soil structure do not come out as the mere summation of strengths and rigidities of soils and geosynthetics. They appear as a result of mechanical interaction between soils and geosynthetics. Ohta et al. (1996, 1998) constructed a series of trial embankments that were reinforced by geosynthetics and tried to examine geosynthetic-reinforcement effect.

This paper aims at numerically examining the geosynthetic-reinforcement mechanism. Herein, the soil which compacted is modeled by the subloading surface Sekiguchi and Ohta's elasto-plastic constitutive model, in which the subloading surface proposed by Hashiguchi (1989) is introduced. This model is capable of expressing the dilatancy characteristics when the current stress state is located inside the yielding surface. The authors believe that the confining effect of the dilative deformation of compacted soils by reinforcements such as geosynthetics would be a key in the reinforcing mechanism.

2. Experiments

2.1 The Used Soil and Preparatory Laboratory Tests

The soil used in experiment is the Pleistocene sand named Omma sand, sampled from Taiyogaoka, Kanazawa, Japan. The specific gravity of soil particle is 2.740, the grain size distribution is the gravel fraction (2 to 75mm) of 2%, the sand fraction (75mm to 2mm) of 80%, the silt fraction (5mm to 75mm) of 11% and the clay fraction (less than 5mm) of 7%, respectively. The uniformity coefficient is 21.8 and the maximum grain size is 9.5mm. In the preparatory laboratory tests, two kinds of soil specimens were prepared: one is completely disturbed (loosened) sample of which water contents were adjusted to prescribed values (25%) as straddling the optimum water content of 18.8%, the other was undisturbed (compacted) sample which was compacted aiming at the optimum water content of 18.8 %.

A series of shear box tests (SBT) were carried out. Both disturbed and undisturbed samples were subjected to shear under the condition of constant volume after completing Ko-consolidation with vertical pressure of 39.2, 78.4, 156.8 and 313kPa. Test results are summarized in Fig. 1 for disturbed (very loosed) sample and in Fig. 2 for undisturbed (compacted) sample. Upper figures indicate the compression curves in Ko-consolidation and lower ones the effective stress paths in shear process under the condition of constant volume. By comparing Figs. 1 and 2, the similarity with saturated clays in both compressibility and dilatancy characteristics can be recog-

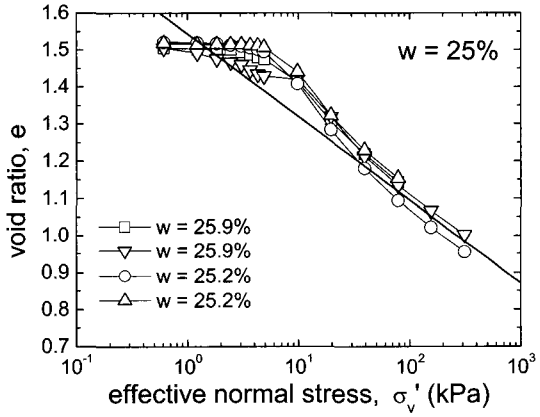

(a) compression lines of disturbed (very loosed) soil specimens

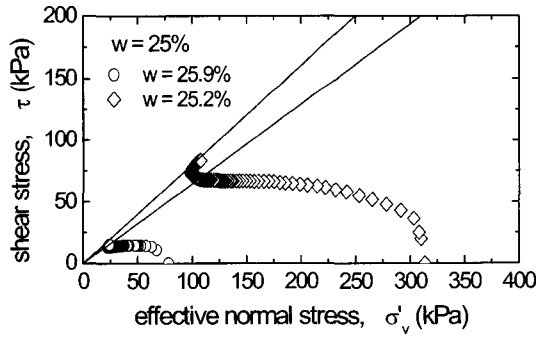

(b) shear properties of disturbed (very loosed) soil specimens

Fig. 1. Mechanical properties of disturbed sample (very loosed) from SBT

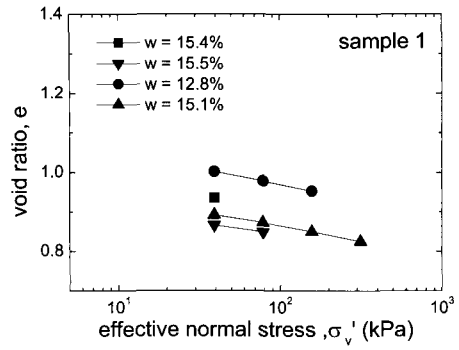

(a) compression lines of undisturbed (compacted) soil specimens

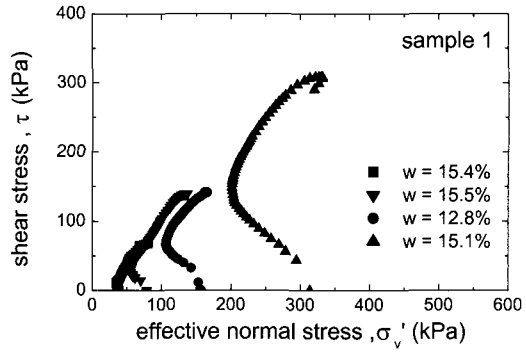

(b) shear properties of undisturbed (compacted) soil specimens

Fig. 2. Mechanical properties of undisturbed (compacted) sample from SBT

nized. Namely, the disturbed (compacted) sample behaves like the overconsolidated clay by contrast with the behavior of disturbed (loosed) sample in normally consolidated clay.

2.2 Compressive Shear Test

The Omma sand with the prescribed water was uniformly compacted by rammer of 3.5kg up to a designated degree of compaction, and it was wrapped by geosynthetics as shown in Fig. 3. The soil was spread in the thickness of 40 to 80mm for each compaction. The compacted soil specimen (30cm in diameter and 40cm in height) was laid on the uniaxial loading apparatus as shown in Fig. 4 and was subjected to compressive shear (Iizuka et al., 2002). Table 1 summarizes the prepared compacted soil specimens for the test. Here, the number of compaction and the spread thickness were varied with the specimen. Some specimens with lower degree of compaction (tests 6 to 8 in Table 1) were also prepared to investigate the influence on the geosynthetic-reinforcement effect due to the difference of the dilatancy characteristics of compacted soil. Herein, in order to measure the extension forces working on geosynthetics, strain gauges are tightly pasted on the geosynthetics as shown in Fig. 3. In the experiment, the vertical displacement of the specimen and the extension stress working on the geosynthetics were measured by using the applied vertical load, as shown in Fig. 4. The compressive shear was carried out at sufficiently slow rate in order to satisfy the condition that the volume of

Table 1. Prepared compacted soil specimens for test

test No	degree of compaction (the number of compaction) ×(layers)	water content w(%)	dry density $\rho_d(g/cm^3)$
2	50×10	18.1	1.53
3	50×10	17.6	1.56
4	50×10	17.3	1.60
5	50×10	17.1	1.54
6	30× 6	16.6	1.43
7	30× 6	17.0	1.43
8	25× 5	16.8	1.45
9	50×10	16.5	1.55

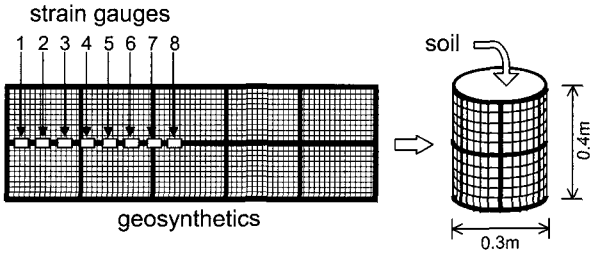

Fig. 3. Strain gauges are installed on geosynthetics to measure extension force

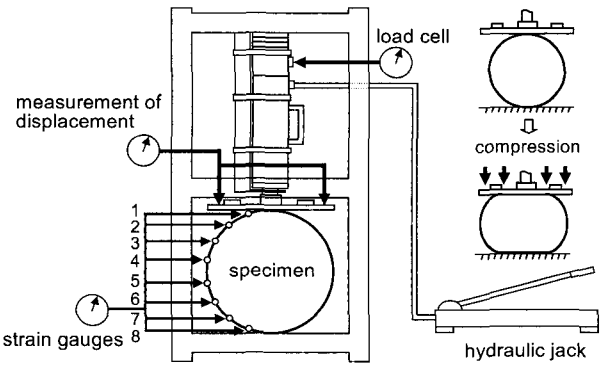

Fig. 4. A schematic of compressive shear apparatus

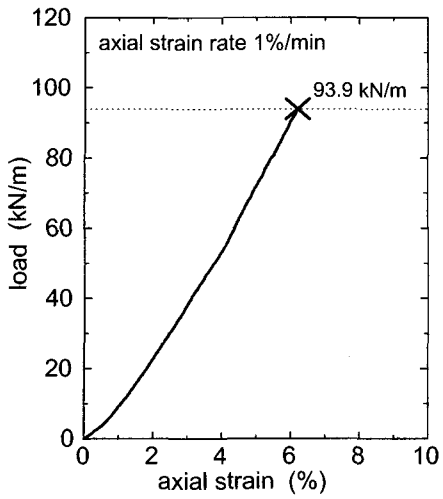

Fig. 5. Stress-strain relation of geosynthetics obtained from uniaxial extension test

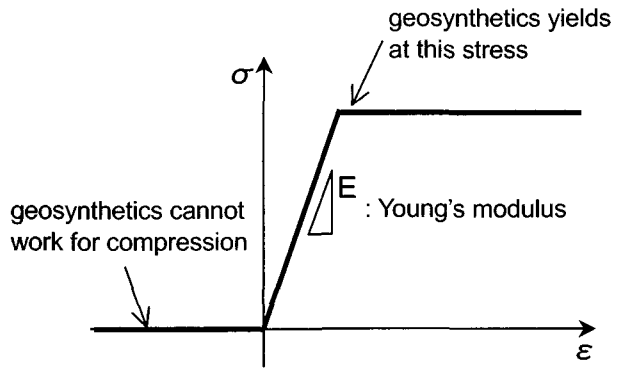

Fig. 6. Geosynthetics model (bar element)

specimen is changeable (drained condition).

In the geosynthetic materials used in the experiment, the uniaxial extension test was carried out to measure the stiffness and the ultimate strength of the geosynthetics. Fig. 5 shows the stress-strain relation of geosynthetic material obtained from the uniaxial extension test. Then, the extension strength is 93.9kN/m, the cross sectional area is $3.2\times10^{-4}m^2$ and Young's modulus is $4.86\times10^{6}kPa$, respectively. Therefore, the geosynthetic has to be modeled as a linearly elastic material as shown in Fig. 6.

3. Elasto-plastic Model of Compacted Soil

In this section, we introduce the conventional elasto-plastic constitutive model (Sekiguchi and Ohta, 1977) and the subloading surface concept (Hashiguchi, 1989) to understand the mechanical behavior inside the normal yielding surface. The constitutive model by Sekiguchi and Ohta (1977) can be regarded as an extension of the original Cam-clay model but is distinguished from the Cam-clay model on description ability of the mechanical behavior, which arose from initial anisotropy and stress reorientation. The determination procedure of input parameters needed in the constitutive model has been well established through a lot of practical case studies using a finite element code, DACSAR, which is employed in the Sekiguchi and Ohta's model (Iizuka and Ohta, 1987; Mestat, 2001).

3.1 Sekiguchi and Ohta's Model with Subloading Surface

The normal yielding function of the Sekiguchi and Ohta's model is expressed as,

$$f=\frac{\lambda-k}{1+e_0}\ln\frac{p'}{p_0'}+D\eta^*-\varepsilon_v^p=0 \tag{1}$$

where D is the coefficient of dilatancy (Shibata, 1968), ε_v^p is the volumetric strain, $\lambda(=0.434C_c)$ and $k(=0.434C_s)$ are the compression and swelling indices, respectively. The parameters of λ, k and D have a theoretical relation with the critical state parameter, M, as $M=\frac{\lambda-k}{D(1+e_0)}$ (Ohta, 1971). η^* is the generalized deviatoric stress parameter, which defined as

$$\eta^*=\sqrt{\frac{3}{2}}\left\|\frac{\mathbf{s}}{p'}-\frac{\mathbf{s}_0}{p_0'}\right\| \tag{2}$$

where $\mathbf{s}$ is the deviatoric stress tensor, the subscript 0 denotes the value at the reference and $\|\cdot\|$ is the Euclid norm. After Hashiguchi (1989), the subloading surface f_s similar to the normal yielding surface can be defined using the similarity ratio R, as,

$$f_s=\frac{\lambda-k}{1+e_0}\ln\frac{p'}{p_0'}+D\eta^*-\left(\varepsilon_v^p+\frac{\lambda-k}{1+e_0}\ln R\right)=0 \tag{3}$$

where the similarity ratio R determines the scale of subloading yielding surface against the normal yielding surface and is defined as $p'/\overline{p'}$ using the current effective mean stress, p' on the subloading yielding

surface and its conjugate effective mean stress, $\overline{p'}$ on the normal yielding surface. The evaluation law of the similarity ratio, $\dot{R}$ is assumed as,

$$\dot{R}=U_R \| \dot{\epsilon}^p \| = -\frac{m}{D}(\ln R) \| \dot{\epsilon}^p \| \quad \text{for} \quad \dot{\epsilon}^p \neq 0 \tag{4}$$

the parameter m is the newly introduced material parameter controlling the accessibility rate of the subloading surface to the normal yielding surface. Herein, note that the scalar function, U_R is defined in the region of $0<R\leq 1$ and satisfies $U_R=\infty$ at $R=0$ and $U_R=0$ at $R=1$.

Since the current effective stress always stays on the subloading surface, the consistency condition can be described as $\dot{f}_s=0$. Therefore, assuming the associated flow rule as $\dot{\epsilon}^p=\Lambda\frac{\partial f_s}{\partial \sigma'}$ and introducing the genera lized Hooke's law for describing the elastic region as $\dot{\sigma}'=D^e\dot{\epsilon}^e=D^e(\dot{\epsilon}-\dot{\epsilon}^p)$, the plasticity multiplier of Λ is determined as,

$$\Lambda=\frac{1}{h}\frac{\partial f_s}{\partial \sigma}\cdot\dot{\sigma}=\frac{1}{H}\frac{\partial f_s}{\partial \sigma}\cdot D^e\dot{\epsilon} \tag{5}$$

$$h=tr\left(\frac{\partial f_s}{\partial \sigma}\right)-mM\frac{\ln R}{R}\left\| \frac{\partial f}{\partial s} \right\|, \text{ and}$$

$$H=h+\frac{\partial f_s}{\partial \sigma}\cdot D^e\frac{\partial f_s}{\partial \sigma} \tag{6)\sim(7}$$

in which, $\dot{\epsilon}$ is the strain increment tensor, $\dot{\sigma}'$ is the effective stress increment tensor and the superscripts of e and p denote the elastic and plastic components, respectively. Therefore, the stress and strain expression of the Sekiguchi and Ohta's model with the subloading surface is obtained as,

$$\dot{\sigma}'=\left[D^e-\frac{\left(K\beta\mathbf{1}+3G\frac{\eta-\eta_0}{\eta^*}\right)\otimes\left(K\beta\mathbf{I}+3G\frac{\eta-\eta_0}{\eta^*}\right)}{\beta^2K+2G+\frac{\dot{p}'}{D}\left(\beta-mM\frac{\ln R}{R}\sqrt{\frac{\beta^2}{3}+\frac{3}{2}}\right)} \right]\dot{\epsilon},$$

$$\beta=M-\frac{3}{2\eta^*}\eta\cdot(\eta-\eta_0) \tag{8}$$

in which D^e is 4th order elastic stiffness tensor, $\mathbf{I}$ is the unit tensor, η is the deviatoric stress ratio tensor ($\eta=\frac{s}{p'}$), β is the accessibility function to the critical state, K is the elastic bulk modulus ($K=\frac{1+e_0}{k}p'$), G is the elastic shear modulus ($G=\frac{3(1-2\nu)}{2(1+\nu)}K$, ν: Poisson's ratio) and $\otimes$ denotes the operator of tensor multiplier. The loading ($\dot{\epsilon}^p\neq 0$) or unloading ($\dot{\epsilon}^p=0$) can be judged by the plasticity multiplier as,

$$\begin{cases}\Lambda<0 : \text{unloading}\\ \Lambda=0 : \text{neutral}\\ \Lambda>0 : \text{loading}\end{cases} \tag{9}$$

Thus the obtained stress and strain relation is installed for input parameters of the finite element code, DACSAR (Iizuka and Ohta, 1987).

3.2 Calibration of the Modeling

In this section, the simulation of shear behavior obtained from SBT under the condition of constant volume is presented. First of all, the input parameters are determined from the compression shear test results for disturbed sample(Fig. 1(a) and (b)). The stress ratio, $(\tau/\sigma'_v)_f$ at the critical state in case of the direct shearing such as the shear box test under the condition of constant volume, can be derived by simultaneously solving the critical state condition, and the undrained (constant volume) condition, $\dot{\epsilon}_v(=\dot{\epsilon}_v^e-\dot{\epsilon}_v^p)=0$ of Sekiguchi and Ohta's model as (Ohta et al., 1993 ; Morikawa et al., 1997),

$$\left(\frac{\tau}{\sigma'_v}\right)_f=\frac{1+2K_0}{3\sqrt{3}}M \tag{10}$$

With empirical relation of $K_0=1-\sin\phi'$ (Jaky, 1944), the critical state parameter, M can be expressed by $(\tau/\sigma'_v)_f$ at $M=\frac{6\sin\phi'}{3-\sin\phi'}$. Here, the experimental value of $(\tau/\sigma'_v)_f$ is given in shear characteristics, though a little difference is found in the critical state lines with the water content. Herein, the kink point of effective stress path is chosen as the critical state point and then the critical state parameter, M is determined to be 1.42. The compression index, $\lambda(=0.434C_c)$ can be directly determined to be 0.12 from compression characteristics of disturbed samples, because it is known that the gradient of compression line from Ko consolidation in

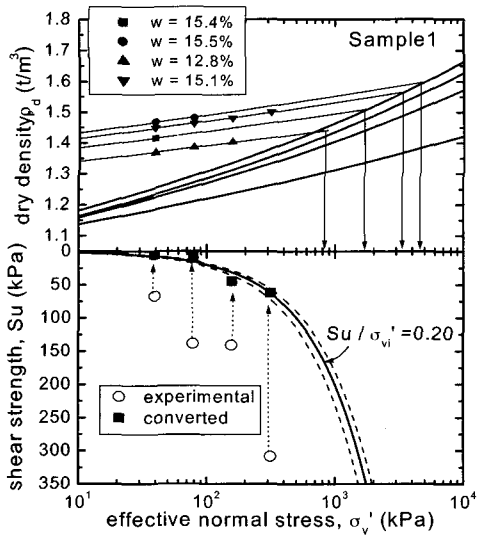

Fig. 7. Estimation of consolidation yield stress

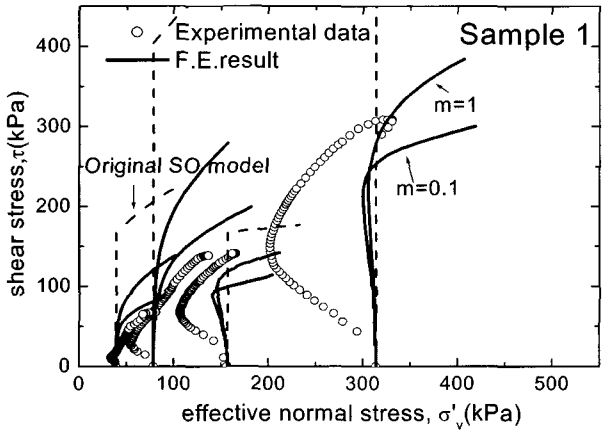

Fig. 8. Computed stress paths of compacted soil obtained from Sekiguchi and Ohta's model with the subloading surface and experimental data

the $e-\ln \sigma_v'$ relation and that from the isotropic consolidation in the $e-\ln p'$ relation coincides with each other (Mitachi and Kitago, 1976). And the swelling index, k is estimated as 0.023 from the empirical relation of $M=1.75(1-\kappa/\lambda)$ (Karube, 1975), since the swelling index required as an input parameter in the constitutive model is the gradient of the isotropic swelling line. But, here, it differs from that of Ko swelling line shown in Fig. 2(a). The equivalent preconsolidation vertical stresses are determined from Fig. 7 with each of water contents. The lateral axis of effective normal stress is rewritten with a logarithm scale and Ko swelling data in Fig. 2(a) are plotted in Fig. 7, together with the compression lines.

The value of equivalent preconsolidation vertical stress is given as each intersection of Ko swelling line and the compression line with each water content value. The equivalent OCR is calculated as $\sigma'_{v0}/\sigma'_{vi}$ from the equivalent preconsolidation vertical stress and the current effective vertical stress. The coefficient of the current earth pressure at rest, K_i is estimated from the empirical relation of $K_i=(OCR)^n K_0$ and n=0.42 (Ladd et al., 1977). Then, the assumed Poisson ratio, ν is 0.33.

The theoretical effective stress paths computed from the Sekiguchi and Ohta's model with the subloading surface using the above-determined input parameters are compared in Fig. 8 with the experimental results of shear characteristics of undisturbed samples, in which the parameters, m defined in Eq.(4) are assumed to be 1.0 and 0.1. And the theoretical paths computed from the original Sekiguchi and Ohta's model without introducing the subloading surface are also compared. It cannot be said that the computed prediction well explains the shear behavior of compacted soil. But at least, it can successfully express the dilatancy characteristics of compacted soil and the case of $m=1.0$ seems to give better prediction for the compacted Omma sand.

4. Finite Element Simulation

4.1 Condition of Analysis and Preliminary Elastic Simulation

A series of finite element simulation of the compressive shear model tests was carried out. Figure 9 shows the finite element modeling of the test, where quadrilateral constant strain element with 4 nodes is

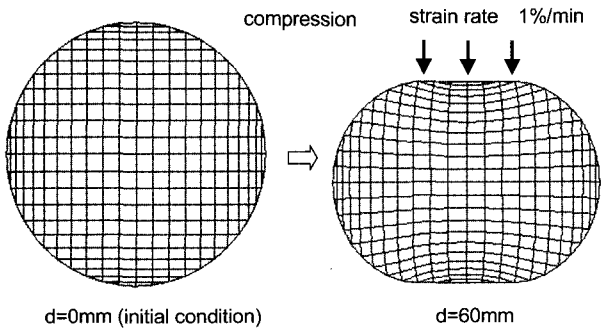

Fig. 9. A schematic of finite element mesh employment

employed. To simulate the compressive shear tests, the displacement is vertically installed to the specimen at the strain rate of 1.0%/min as indicated in Fig. 9.

To begin with, as a preliminary simulation, the compacted soil is regard as a linearly elastic material that has no irreversible dilatancy characteristics associated with shearing. And also, based on the uniaxial extension test result of geosynthetics (Fig. 5), the geosynthetics wrapping the soil specimen is modeled by linear elastic bar elements as shown in Fig. 6. The properties are the Young's modulus of $E=4.86\times10^{6}$kPa, the cross sectional area of $A=3.2\times10^{-4}m^2$ and the compression strength of N_f=93.9kN/m, respectively. In the computation, it is assumed that the bar elements (modeling the geosynthetics) do not resist against the axial compression as indicated in Fig. 6.

Figure 10 compares the load and displacement relation obtained from the experiments with the computed ones. Here, three values of the Young's modulus for the compacted soil are chosen as shown in the figure, but the Poisson's ratio is uniquely assumed to be 0.33 in all cases. The case of E=6000 kPa seems to well explain the load and displacement relation of well-compacted specimen, test 5 (see, Table 1). The change of cross sectional area and circumference length of specimen are compared in Figs. 11 and 12, respectively. The Young's modulus of 6000 kPa is used in the computation because the case well explains the load and displacement relation, but the poisson's ratio is varied from 0.2 to 0.499 for various cases. As for the change of cross sectional area of the specimen in Fig. 11, all the cases can be described as the tendency showing the experiments(decrease of cross

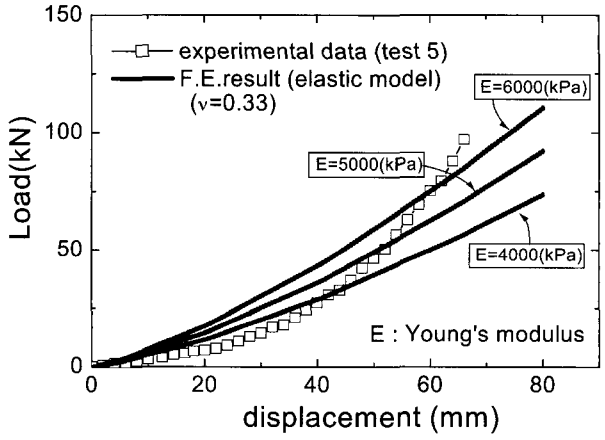

Fig. 10. Computed load and displacement relation with experimental result

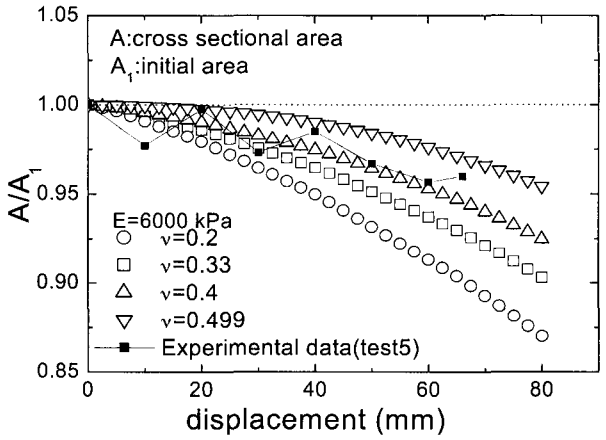

Fig. 11. Computed cross sectional area for various Poisson ratio (elastic model)

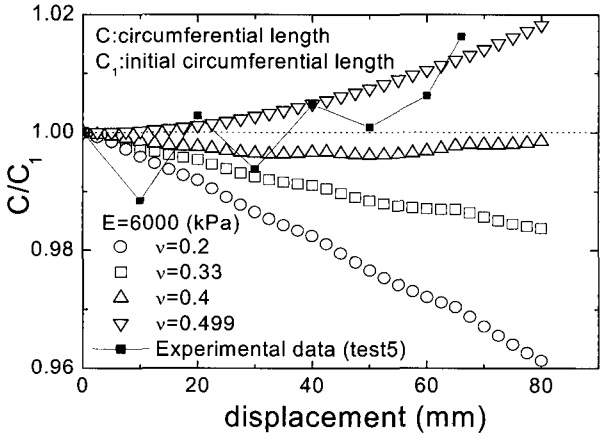

Fig. 12. Computed circumference length for various Poisson ratio (elastic model)

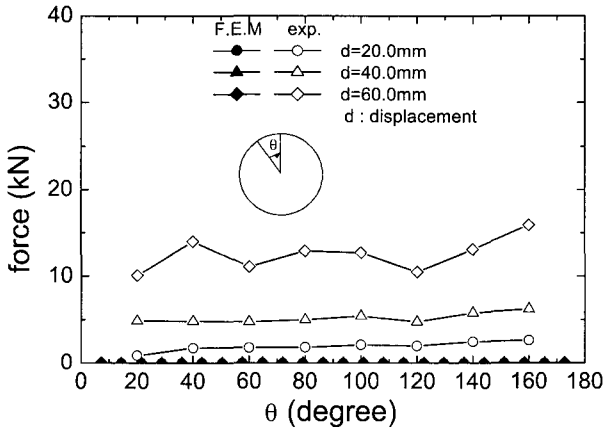

Fig. 13. Extension forces along circumference of specimen (elastic model) (E=6000 kPa and ν=0.33 for test5)

sectional area with loading). However, for the change of circumference length of the specimen as shown in Fig. 12, only the case of ν=0.499 can explain the experimental result of test 5. The assumption of ν=0.499 theoretically means the almost incompressibility condition and cannot be accepted as the poisson ratio of soil materials in the engineering practice. Figure 13 compares the computed distribution of extension forces working to the geosynthetics with the measured ones in test 5. From the figure, the elastic assumption without considering the dilatancy characteristics during the compressive shearing for the compacted soil cannot explain the geosynthetic-reinforcement effect observed in the model test.

4.2 Elasto-plastic Finite Element Simulation

The material parameters needed in the elasto-plastic modeling of the compacted soil was already determined in the previous section. Now, it is necessary to estimate the equivalent preconsolidation vertical stresses in the compressive shear model tests. Figure 14 indicates the procedure to estimate the equivalent preconsolidation vertical stress considering the water content.

Since the evaluation of the initial effective vertical stresses in the specimen just before the compressive shear in the model test was very difficult, the equivalent preconsolidation vertical stress was determined as the value corresponding to the initial dry density of each specimen as shown in Fig. 7, which was not considered

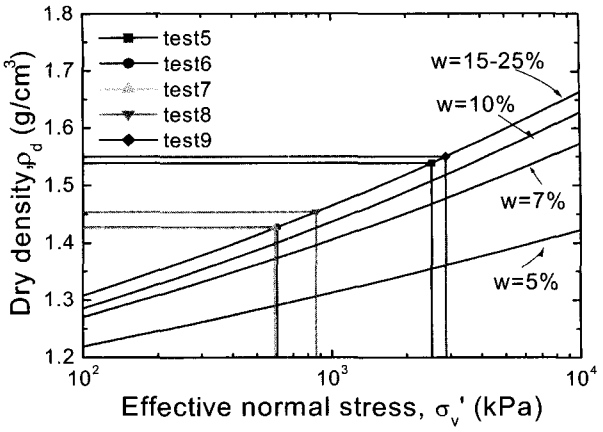

Fig. 14. Estimate of equivalent preconsolidation stress with water content

the slope of swelling line. Although the initial effective vertical stress, in reality, would not be uniform but is distributed in the specimen, the effective overburden pressure estimated at the center of specimen is employed in the computation as a representative value.

Figure 15 compares the computed load and displacement relation with the experimental results. In the figure, the black symbols, FEM 5 and FEM 9, denote the cases of well compacted specimen (high degree of compaction), corresponding to Test 5 and Test 9, respectively, while white symbols, FEM 6, FEM 7 and FEM 8, represent the cases of relatively poorly compacted specimen (relatively low degree of compaction), corresponding to Test 6, Test 7 and Test 8, respectively. Although the complete agreement between the computed and the measured results cannot be seen, it is found that the

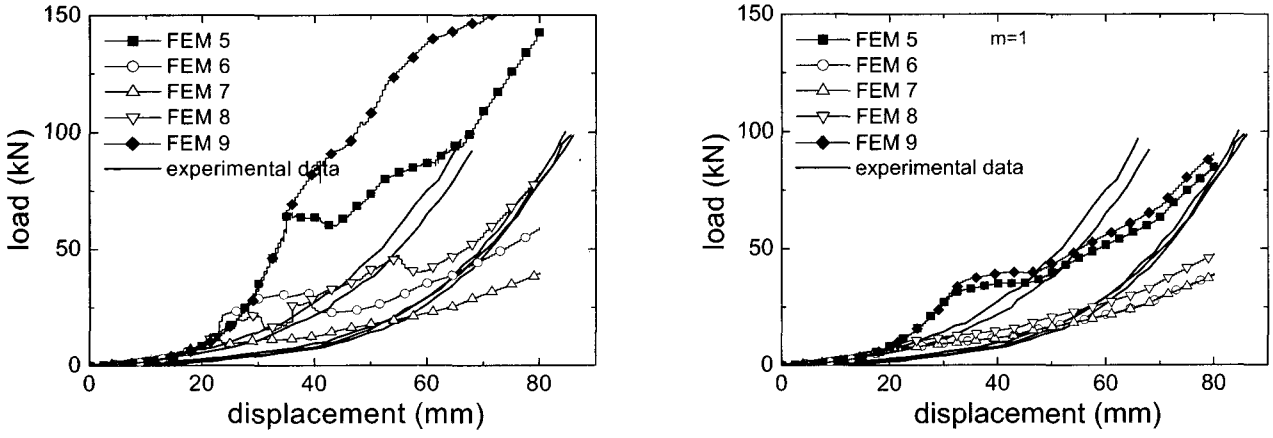

(a) Original Sekiguchi and Ohta's model

(b) Subloading model with m=1

Fig. 15. Computed load and displacement relation with experimental result

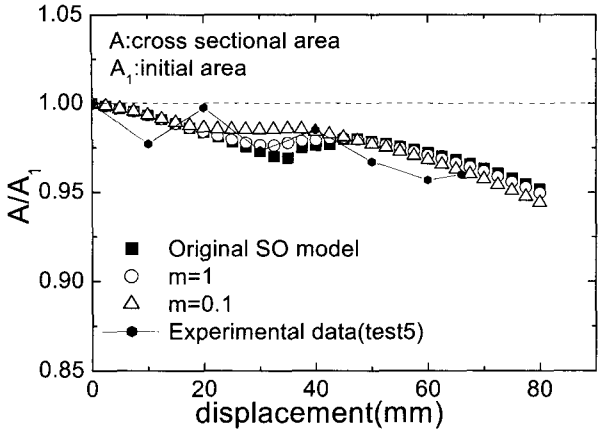

Fig. 16. Computed cross sectional area

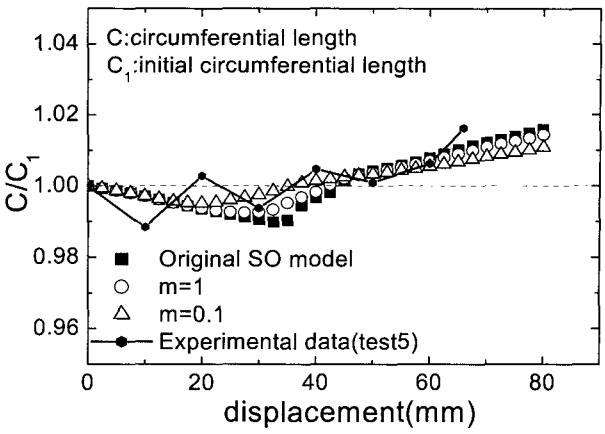

Fig. 17. Computed circumference length

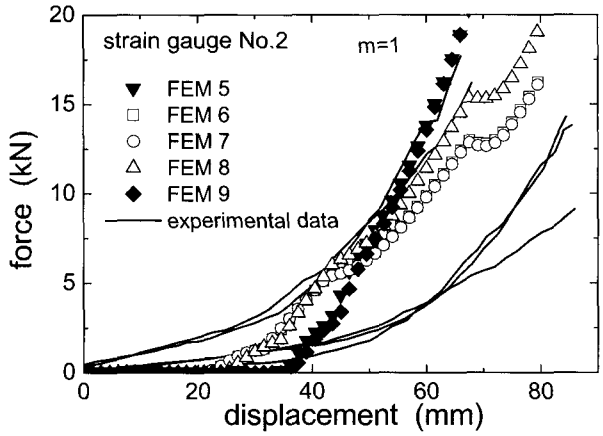

Fig. 18. Extension forces working on the geosynthetics with the displacement at the location for NO.2 strain gauge

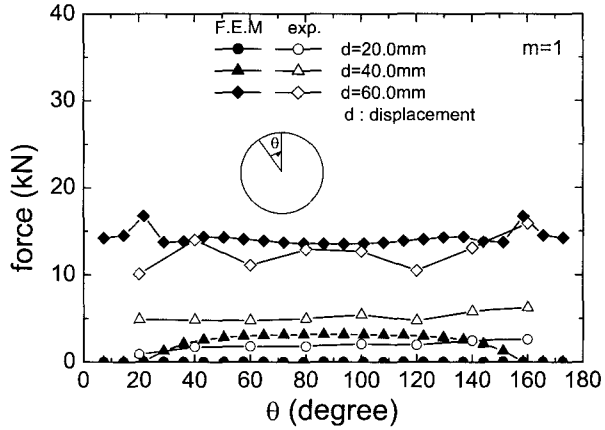

Fig. 19. Extension forces along circumference of specimen (Test5)

computed results, at least, explain the influence due to the difference of compaction degree. Moreover, it is found that introducing the subloading surface inside the normal yielding surface brings about smoother development of load and displacement curves, similar to the experimental results. Especially, the case of $m=1.0$, which controls the accessibility rate of the subloading surface to the normal yielding surface as defined in Eq.(4), seems to give better prediction.

Figs. 16 and 17 compare the computed cross sectional area and circumference length of the specimen with the measured results (test 5). It can be seen that the computed predictions well explain the measured results.

Figure 18 indicates the computed development of axial forces working on the geosynthetics with the displacement at the locations of the strain gauges No.2 and compared with the measured results. And, Figure 19 shows the computed distribution of axial forces along the circumference of the specimen, in which the case of high compaction degree (Test 5, FEM 5) is shown in Fig. 15.

5. Conclusions

This paper presents the methodology and the tool to analyze the geosynthetic-reinforced soil structures and discusses the confining effect due to the geosynthetics wrapping the compacted soil specimen by conducting a series of the compressive shear model tests and the finite element simulations. Particularly, the mechanical interaction between the compacted soils and the geosynthetic-reinforcement materials is emphasized as a benchmark that should be taken into consideration in analyzing the geosynthetic-reinforcement effect. Major items presented in this paper are summarized as follows.

(1) The dilatancy characteristics of compacted soils depending on the degree of compaction are discussed. A trail to quantitatively express the degree of compaction by introducing the equivalent preconsolidation stress is presented.

(2) The elasto-plastic constitutive modeling with the subloading surface is introduced to describe the mechanical behavior of compacted soils and its applicability to the compacted soils is examined.

(3) A series of compressive shear tests for the compacted soil specimens wrapped by the geosynthetics is carried out and the geosynthetic-reinforcement effect is also examined.

(4) A series of elasto-plastic finite element simulation of the compressive shear tests is performed and the applicability of the simulation technique to the analysis of the geosynthetic-reinforcement mechanism is examined by comparing the computed prediction with the measured results.

Acknowledgements

The authors acknowledge Professor Atsushi Iizuka and Instructor Katsuyuki Kawai, Kobe University for their continuous encouragement to this research.

References

1. Hashiguchi, K. (1989), "Subloading Surface Model in Unconventional Plasticity", *Int. J. of Solids and Structures*, Vol.25, pp. 917-945.
2. Iizuka, A. and Ohta, H. (1987), "A Deformation Procedure of Input Parameters in Elasto-Viscoplastic Finite element analysis", *Soils and Foundations*, Vol.27, No.3, pp.71-87.
3. Iizuka, A., Hirata, M., Yokota, Y., Ohta, H., Kim, E.R., and Kubo, T. (2002), "Compressive Shear Tests of Compacted Soils Wrapped by Geosynthetics", *Proc. of 7th International Conference on Geosynthetics*, IGS, Vol.3, pp.1133-1136.
4. Jaky, J. (1944), Tarajmechanika, *Journal of Hungarian Architecture and Engineering*, pp.355-358 (in Hungarian).
5. Karube, D. (1975), "Unstandardized Triaxial Testing Procedures and Related Subjects for Inquiry", *Proc. of 20th Symposium on Geotechnical Engineering*, pp.45-60 (in Japanese).
6. Ladd, C.C., Foott, R., Ishihara, K., Schlosser, F., and Poulos, H.G. (1977), "Stress-Deformation and Strength Characteristics", *Proc. of 9th International Conference on Soil Mechanics and Foundation Engineering*, Vol.2, pp.421-494.
7. Mestat, P. (2001), MOMIS: A Database for the Numerical Modelling of Embankment on Soft Soils and the Comparison between Computational Results and In-situ Measurements, *Bulletin des Laboratories des Ponts et Chaussees*, Vol.232, Ref 4376, pp.45-60.
8. Mitachi, T. and Kitago, S. (1976), "Change in Undrained Shear Strength Characteristics of Saturated Remolded Clay due to Swelling", *Soils and Foundations*, Vol.16, No.1, pp.45-58.
9. Morikawa, Y, Furuta, Y., Iizuka, A., and Ohta, H. (1997), "Constant Volume Shear Strength of Clayey Soils", *Journal of Geotechnical Engineering*, JSCE, No.582/III-41, pp.173-182 (in Japanese).
10. Ohta, H. (1971), "Analysis of Deformation of Soils Based on the Theory of Plasticity and Its Application to Settlement of Embankments", *Thesis of Doctor of Engineering, Kyoto University.*
11. Ohta, H. and Hata, S. (1977), "Strength of Dynamically Compacted Soils", *Proc. of 9th International Conference on Soil Mechanics and Foundation Engineering*, Tokyo, Vol.1, pp.239-242.
12. Ohta, H., Nishihara, A., Iizuka, and A., Sugie, S. (1993), "Vane Strength in Anisotropically Consolidated Clay Deposits", *Journal of Geotechnical Engineering*, JSCE, No.481/III-25, pp.145-154 (in Japanese).
13. Ohta, H., Goren, S., Iizuka, A., Yamakami, T., Yamagishi, K., and Moroto, N. (1996), "Numerical Simulation of Beam-Shaped Soil Structure Reinforced by Geosynthetics", *Proc. Of Int. Symposium on Earth Reinforcement*, Balkema, Vol.1, pp.255-260.
14. Ohta, H., Hirata, M., Iizuka, A., Yamakami, T., Yokota, Y., and Ohmori, K. (1998), "Application of Dilatancy Models to Soils Reinforced by Geosynthetics", *Sixth International Confernce on Geosynthetics*, pp.551-556.
15. Sekiguchi, H. and Ohta, H. (1977), "Induced Anisotropy and Time Dependency in Clays", Proc. Specialty Session 9, *9th International Conference on Soil Mechanics and Foundation Engineering*, Tokyo, pp.229-239.
16. Shibata, T. (1968), "On the Volume Change of Normally Consolidated Clays", *Technical Report of Disaster Prevention Research Institute*, Kyoto University, Vol.6, pp.128-134 (in Japanese).

(received on Feb. 9, 2004, accepted on Apr. 12, 2004)